ON THE SPECTROGRAPHIC REPRESENTATION OF CARDIOVASCULAR FLOW INSTABILITIES*

Thangam Natarajan*[1], Daniel E. MacDonald*[1], Mehdi Najafi[1], M. Owais Khan[2], and David A. Steinman[1]

[1]Biomedical Simulation Lab, Department of Mechanical & Industrial Engineering
University of Toronto, Toronto, Ontario, Canada
[2]Department of Pediatrics, Stanford University, Stanford, USA
* indicates co-first authorship.

ABSTRACT

In the past decade, high-fidelity computational fluid dynamics (CFD) has uncovered the presence of high-frequency flow instabilities (on the order of 100 s of Hz) in a variety of cardiovascular applications. These fluctuations are typically reported as pulsatile velocity-time traces or fast-Fourier-transformed power-frequency spectra, often from a single point or at most a handful of points. Originally inspired by its use in spectral Doppler ultrasound, here we demonstrate the utility of the simplest form of time-frequency representation—the spectrogram—as a more comprehensive yet still-intuitive means of visualizing the potential harmonic complexity of pulsatile cardiovascular flows. After reviewing the basic theory behind spectrograms, notably the short-time Fourier transform (STFT), we discuss the choice of input parameters that inform the appearance and trade-offs of spectrograms. We show that spectrograms using STFT were able to highlight spectral features and were representative of those obtained from more complex methods such as the Continuous wavelet transforms (CWT). While visualization properties (colourmap, filtering, smoothing/interpolation) are shown to affect the conspicuity of spectral features, the window properties (function, size, overlap) are shown to have the greatest impact on the resulting spectrogram appearance. Using a set of cerebral aneurysm CFD cases, we show that spectrograms can readily reveal the case-specific nature of the time-varying flow instabilities, whether broadband, suggesting intermittent turbulent-like flow, or narrowband, suggesting laminar vortex shedding, or some combination thereof.

Keywords Flow instabilities · High-frequency fluctuations · Spectrogram · STFT · Time-frequency representation

1 Introduction

Recent high-fidelity computational fluid dynamics (CFD) studies have reported high-frequency flow instabilities, on the order of 100's of Hz, for a range of cardiovascular applications, including the heart [1], arteriovenous fistulae [2], carotid stenoses [3] and cerebral aneurysms [4]. The presence of high-frequency velocity fluctuations has been known to cause degenerative changes in vascular pathology including endothelial or mural cell remodeling and turnover [5, 6, 7, 8]. Measuring and characterizing these flow fluctuations is imperative to better understand the various pathophysiological mechanisms and their disease progression. These fluctuations are typically presented as point-wise measurements, i.e. velocity–time traces, and/or transformed to the frequency domain and presented as power spectra. Such representations have two major drawbacks. First, being point-wise data, they are inadequate for construing the global behavior of what are typically spatially heterogeneous flows. Second, algorithms such as fast Fourier transforms (FFT) are not well suited to pulsatile velocity data, since they may blur or mask harmonic content that can vary over the cardiac cycle.

Citation: This article has been accepted for publication in *J Biomech* 110, p.109977 (2020) following peer review, and the Version of Record can be accessed online at https://doi.org/10.1016/j.jbiomech.2020.109977.

Various techniques have addressed these drawbacks, to different degrees. The short-time Fourier transform (STFT), among others, has commonly been used in depicting the time–frequency representation (TFR) by performing FFTs over short consecutive subsets of the signal. This method, whilst being simple and computationally inexpensive, assumes that the analyzed signal is stationary for a short interval of time, and high resolution in time or frequency may be achieved at the expense of each other. Continuous wavelet transforms (CWT) use multi-resolution (variable width) 'wavelets' to negate this limitation of the STFT, allowing better localization of frequency components in time, but requiring the mother wavelet to be representative of the signal being analyzed. More complex modal spectral analyses (see [9]) exist such as spectral proper orthogonal decomposition (SPOD) and dynamic mode decomposition (DMD) that provide time-harmonic modes at discrete frequencies through a discrete Fourier transform (DFT). While these methods perform exceedingly well in extracting coherent structures of a statistically stationary flow, they share more commonalities with the DFT, and thus the localization of frequencies in time is missing [10, 11]. Moreover, they can be computationally inefficient on translation to a clinical workflow.

Therefore, we propose the use of short-time Fourier transform (STFT) and a particular type of TFR—the spectrogram—for its conceptual simplicity and its intuitive connection to the clinic and clinicians, i.e., Doppler ultrasound spectrograms. We also demonstrate that the spectrograms obtained through STFT are representative of the CWT while being simpler and computationally less expensive.

In the broadest sense, a spectrogram is a visual representation of the evolution of spectral content of time series data, essentially mapping the power of the signal to colour and/or intensity in a time–frequency (t-f) plane. While TFRs have been used extensively in biomedical signal analyses, for instance, electroencephalography (EEG) [12], Doppler blood flow signals [13], electrogastrography (EGG) [14], in vitro experiments of aortic valve regurgitation [15], their potential utility for elucidating the broad characteristics of unstable flow phenomena in cardiovascular flows seems to have been overlooked. This is likely because the prevalence of high-frequency flow fluctuations has only recently been evidenced by cardiovascular CFD, and, although the generation of spectrograms seems superficially straightforward, there are numerous parameters and decisions involved in generating satisfactory depictions.

To encourage adoption of a rich but still-intuitive representation of flow instabilities, here we revisit the formulation of a 'conventional' spectrogram from velocity time series data obtained from high-resolution CFD simulations, focusing on cerebrovascular flows where these instabilities may be particularly prevalent, and defy simple classification as laminar or turbulent [16, 17]. We provide rationales for objectively choosing parameters to generate faithful representations of the spectral content when displayed as TFRs and, in the process, clarify the sensitivity and trade-offs of TFRs to CFD and input parameters. Finally, we demonstrate the utility of spectrograms for visualizing and discriminating spectral characteristics from a set of cerebral aneurysm CFD cases.

2 Materials and Methods

The linear transformation of a time-varying, non-stationary data to the frequency domain is performed using STFT. The STFT of a time series data, defined as,

$$X_l(k) \triangleq \sum_{n=0}^{N-1} x(n+lH)w(n)e^{-i\frac{2\pi kn}{N}}, l = 0, 1, ..., L \tag{1}$$

is applied to the raw data, which is essentially a discrete Fourier transform at every frame l with a sliding window function $w(n)$ advancing per time increment H (hop size), with $k \in [0 : K]$, where $K = N/2$ is the frequency index corresponding to the Nyquist frequency and N the length parameter that determines the duration of the considered section. The final frame L depends on the hop size and the window length (number of samples). The windowed STFT results in preserving the temporal information (as opposed to a conventional FFT) and attenuates spectral leakage that arises due to signal discontinuities. The STFT results in the magnitude and phase alone the frequency axis at each windowed frame.

The power spectral density (P_l) of each frame is then obtained by taking its magnitude squared as,

$$P_l(k) = \frac{1}{\sum_{n=0}^{N-1} |w(n)|^2} |X_l(k)|^2 \tag{2}$$

A spectrogram S can then be generated simply by displaying the logarithm of the power (to reduce the dynamic range) as colour and/or intensity at each windowed time frame (x-axis) and its frequency bins (y-axis).

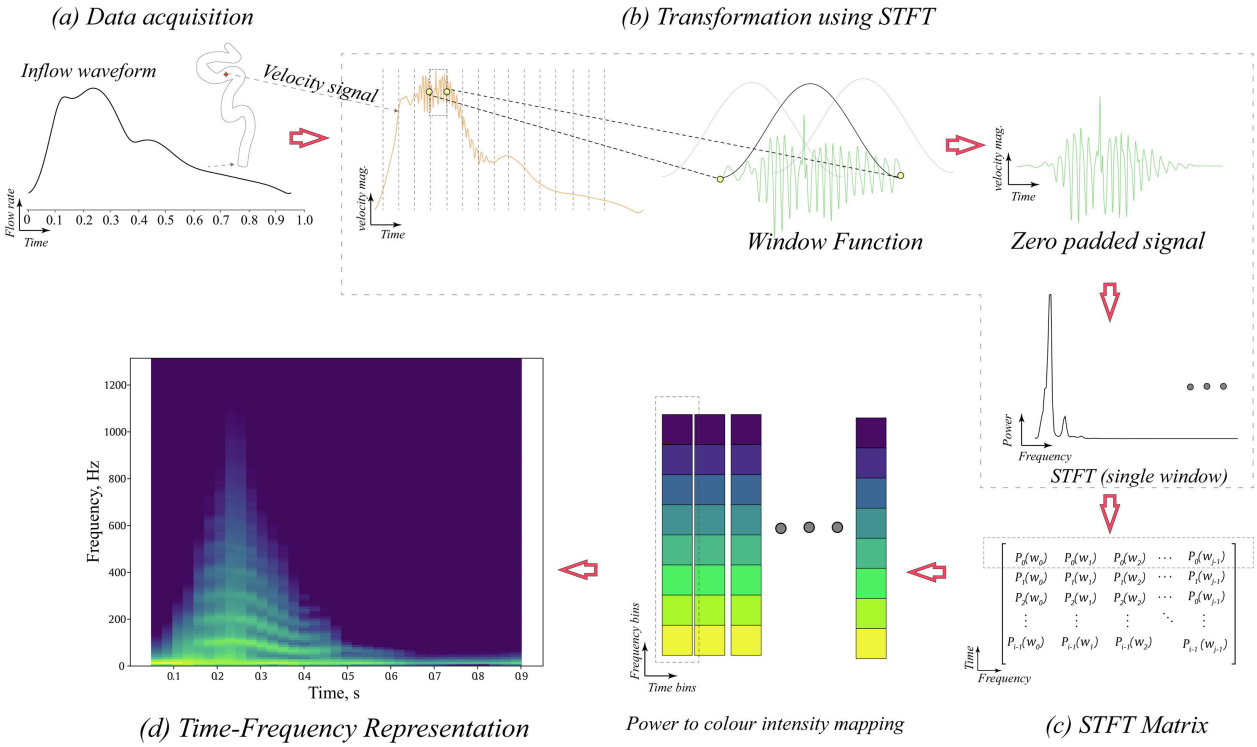

Figure 1: Illustration of the spectrogram generation process: (a) Data acquisition–acquiring time series data from a 3D CFD data, showing the driving inflow waveform; (b) Transformation using STFT–applying suitable window function, window length to obtain the power spectra; (c) Power spectra arranged as STFT matrix where the logarithm of power is mapped to intensity; and (d) The resulting "classical" spectrogram or TFR.

As illustrated in Fig. 1, transformation using STFT involves selecting a suitable windowing function that has: minimal spectral leakage; a window length that determines the time and frequency resolution; and a window overlap (in combination with window length) that determines the smoothness/smearing of the resulting spectrogram. As demonstrated and discussed below, the choice of functions and parameters can have a dramatic effect on the spectrogram appearance. The reader is referred to the more exhaustive reviews for detailed aspects of the mathematical formulations [18, 19].

For these demonstrations, we use high-resolution CFD datasets of anatomically realistic (medical-imaging-derived) cerebral aneurysms and an internal carotid artery siphon model from the open-source AneuriskWeb project database (2012) [20]. The meshing, solver, and simulation methodology are detailed elsewhere [21]. The strategies presented herein assume the solution of the dataset has been properly verified; the requirements for that are beyond the scope of the paper [17, 22].

3 Results

3.1 Advantages of STFT over CWT for cardiovascular flows

Fig. 2 shows the global spectrograms (discussed in detail later) from five aneurysm CFD cases computed by STFT and CWT respectively. For each model, the STFT spectrograms were generated using all the points (∼600,000 points on an average) and using 2500 time-steps over the cardiac cycle. CWTs were computed using equivalent temporal resolution but using only 2500 randomly selected points for reasons of computational efficiency, as discussed later. The spectrogram using STFT was computed with a Hann window function with a length N chosen to produce 10 non-overlapping windows and a hop size determined by a choice of 75% overlap, resulting in a frequency resolution of 10 Hz and a time resolution of 0.026 s. For the CWT, the complex Morlet wavelet function was used as it is the closest representation of the velocity signal. In both cases, the logarithm of the power is used to reduce the dynamic range and is mapped to colour intensity after being thresholded at -20 dB.

First, looking at the gross features of power, it is clear that C0004 and C0053 have strong, high-frequency fluctuations up to ∼1 kHz. In all these cases the instabilities develop and persist throughout systole and then return, with varying

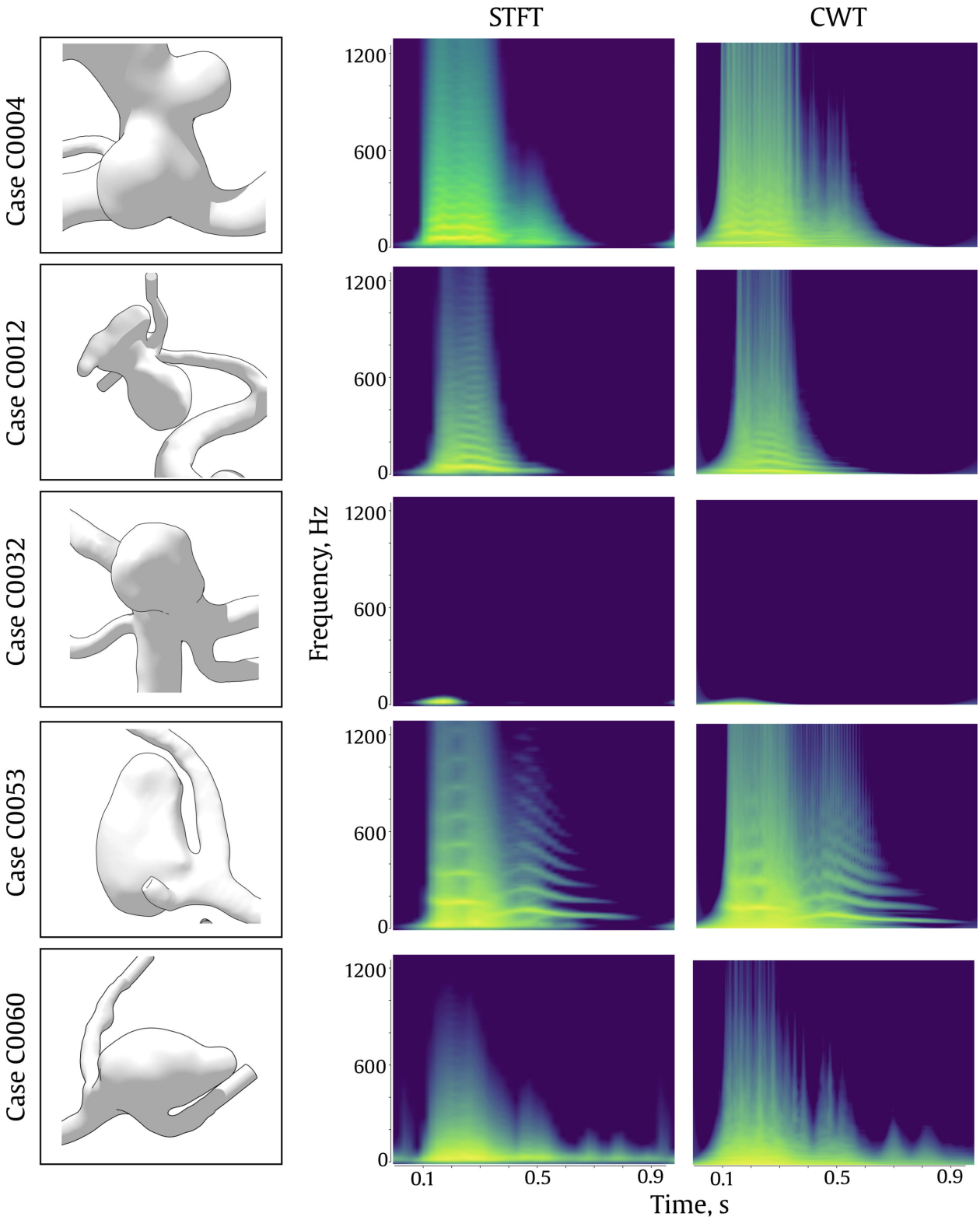

Figure 2: Comparison of spectrograms computed through STFT and CWT for five aneurysm cases (0004, 0012, 0032, 0053 and 0060 from AneuriskWeb project database).

strength, during the mid-diastolic phase beginning after the dicrotic notch (c.f. Fig. 1a). On the other hand, case C0060 is characterized by high-frequency fluctuations that nevertheless, persistent deep into the cardiac cycle, while C0032 shows no high-frequency fluctuations at all. Looking beyond the "envelope" of the spectrogram to the details within, we see in cases C0004, C0012 and C0053 evidence of narrowband features (i.e., horizontal striations) that repeat at regular frequency (vertical) intervals, suggestive of periodic or near periodic flow phenomena like laminar vortex shedding. In C0004 and C0012 they arise only during systole (with a fundamental frequency $\sim$50 Hz). In C0053, on the other hand, they arise during systole (with fundamental frequency $>$ 200 Hz); are briefly smeared into smoother, more broadband features suggestive of disordered or turbulent-like flow; and become narrowband again past the dicrotic notch, albeit at a lower fundamental frequency that is further decreasing in time.

It is evident that the spectral representations of both STFT and CWT are similar although minor differences can be observed at higher frequencies due to the multi-resolution nature of CWT. In general, the inter-aneurysm differences outweigh the differences between the STFT and CWT. The STFT, while providing nearly an exact representation of the CWT, was computationally faster by at least an order of magnitude ($\sim$120 s vs. $\sim$1200 s on a modern Desktop workstation) i.e. considering all the points for the STFT and only 2500 points for the CWT. The computational efficiency also scaled non-linearly with the number of points; While CWTs may be efficient for high spectral resolution within a handful of points, STFTs seem to be better suited, at least from a practical and clinical standpoint, for cases where several thousand points may need to be taken into consideration. Therefore, given its innate simplicity and efficiency, the rest of the Results focus on the STFT.

3.2 Parameter selection and sensitivity

The appearance of TFRs generally, and STFTs specifically, depends on a number of user-selectable parameters. Below we demonstrate the sensitivity of TFRs to these, in order to inform their optimal selection for the rest of the Results.

3.2.1 Number of time points, time & frequency bounds

With numerical studies, the number of stored time-step data ("snapshots") indirectly dictates the Nyquist frequency (folding frequency) beyond which the spectra cannot be represented in the TFR. Assuming the snapshots are saved at regular intervals, the sampling rate f_s is given by N/T where N is the number of snapshots and T is the period of sampling (here, T corresponds to the period of one cardiac cycle, equal to 0.951 s). For instance, a dataset simulated with 10,000 time-steps per cardiac cycle would, in principle, allow us to analyze frequencies up to 5.3 kHz (recall that the reported frequency range observed in cerebrovascular flows is on the order of 100 s of Hz [23, 24, 16]), and the sampling rate would be f_s = 10.5 kHz. In practice, however, snapshots are typically saved for only a subset of (typically equal-spaced) time-steps in order to minimize storage and reduce I/O bottlenecks. In our cases we typically write only 1250-2500 snapshots/cycle, i.e., allowing to resolve frequencies up to 0.6-1.3 kHz.

3.2.2 Window length, functions & overlap

Fig. 3 shows the sensitivity of window length, window functions, and the percentage overlap on the resulting appearance of the spectrogram for a carotid siphon model (C0006) from Valen-Sendstad et al., 2014. This siphon model had a flow that was laminar and stable but showed strong vortex shedding for $\sim$250 ms. As the STFT assumes the time series data to be short-time stationary within the span of the analysis window, the window length is certainly the most important parameter to be set: a longer window length (therefore fewer windows through time) provides higher frequency resolution at the expense of poorer time resolution, and vice versa for shorter windows. An ideal window size would thus be one that resolves both time and frequency satisfactorily. The choice of a windowing function is determined by two spectral characteristics: width of the main lobe, and the peak side-lobe level [25]. An ideal analysis window would have a narrow main lobe to minimize spectral smoothing (good frequency resolution/minimal smoothing) and very low side-lobes (reduced spectral leakage), such as a Hann window that is conventionally considered a safe option for most applications [26]. Effects of other commonly used window functions such as the Tukey, Hamming and Blackman are shown in Fig. 3 as well. The percentage overlap essentially determines the additional spectral frames between two non-overlapping windows. A 75% overlap is generally recommended as a compromise between spectral resolution and smearing [27] although some studies have utilized 50% [28, 1]. In summary, an optimal set of parameters for the cases under consideration here would be, for instance, considering the length of the time-series data to be for 0.951 s and 2500 snapshots in time, to arrive at 10 non-overlapping windows, the window length would be 250 samples, then zero-padded to 256 (i.e. window length = snapshots/ no. of windows). Due to the nature of the FFT, it is customary to choose window lengths, or pad with zeros, to the closest power of 2 (i.e. 256 instead of 250). A 75% overlap would result in $0.75 \times 256 = 192$ samples (3 overlapping windows between 2 non-overlapping windows) amounting to a total of 36 spectral windows. This results in a frequency resolution of 10 Hz and a time resolution of 0.026 s.

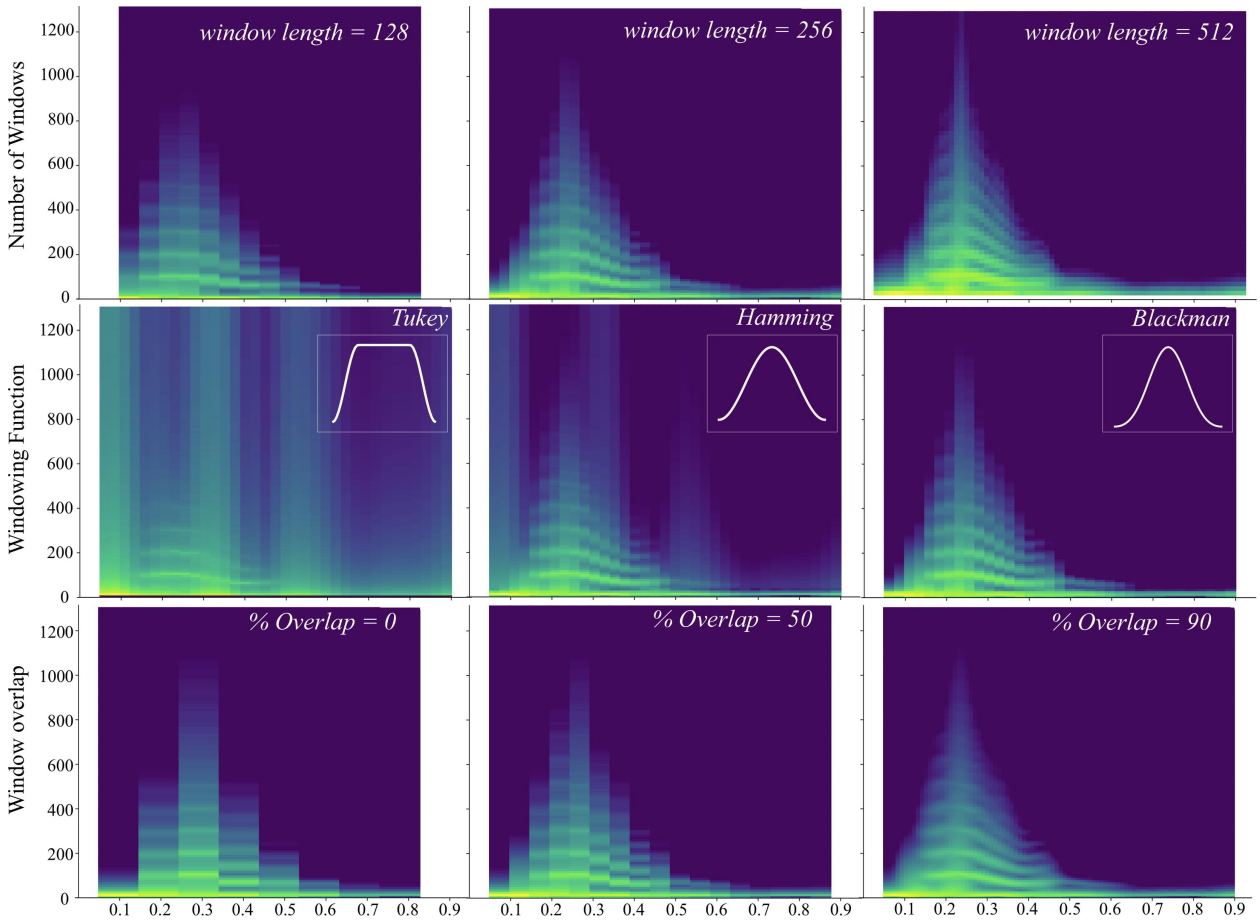

Figure 3: Effect of windowing-parameters on spectrograms–for each row, all other variables (other than mentioned) are held constant. Note the different time (x-axis) extents, since these depend on the window parameters.

3.2.3 Region of interest (local and global spectrograms)

Ultimately, the spectrograms are constructed by averaging the STFT power spectra from some or all of the nodal velocity-time data within the CFD model domain. For instance, in Fig. 4, the model of a cerebral aneurysm (Case C0078) is partitioned into sub-regions (I through V) where local spectrograms (Fig. 4a) may be obtained from each of these sub-regions or a global spectrogram averaged over the entire domain (Fig. 4b). Fig. 4c shows the simple FFT power spectral density averaged in each of these regions, which indicates that nearly all (99%) the energy is concentrated below 25 Hz, which are in fact those of the driving pulsatile inflow waveform [29]. From Fig. 4a, it is seen that the local spectrogram of the sac region (Region-V) and the global spectrogram are considerably similar, a consequence of the fact that (in this case at least) much of the vasculature proximal to the sac (Regions I-III) is dominated by the low frequencies of the driving flow waveform, reflected in the bright spectral bands below 25 Hz whereas the bulk of the high-frequency spectral content is generated within, and to a lesser extent, just proximal to the sac (also evident through velocity-time traces in Fig. 4d).

3.2.4 Choice of colourmaps & dynamic range

The colourmaps used in diagnostic tasks (especially in a clinical setting) often have a non-negligible impact on the decision outcome (see [30, 31]). Fig. 5 shows the spectrogram with the inset TFRs showing the highlighted region with some of the commonly used colourmaps. The line plot shows the variation in the perceptual deltas (derivatives of perceived change in colour) for each of the colourmaps used. A commonly used Hue, Saturation, Intensity (HSI) colourmap such as 'jet' or a 'rainbow' can exaggerate/suppress the features and alter the visual perception of spectra. It is recommended to use a perceptually uniform colourmap (such as cividis [32], viridis in matplotlib [33] or parula in MATLAB[34]) to remove the bias of the perceived change [32]. In the cerebrovascular flows considered here, it also may be instructive to remove the inflow 'carrier' ($<$25 Hz) from the time series data in some circumstances

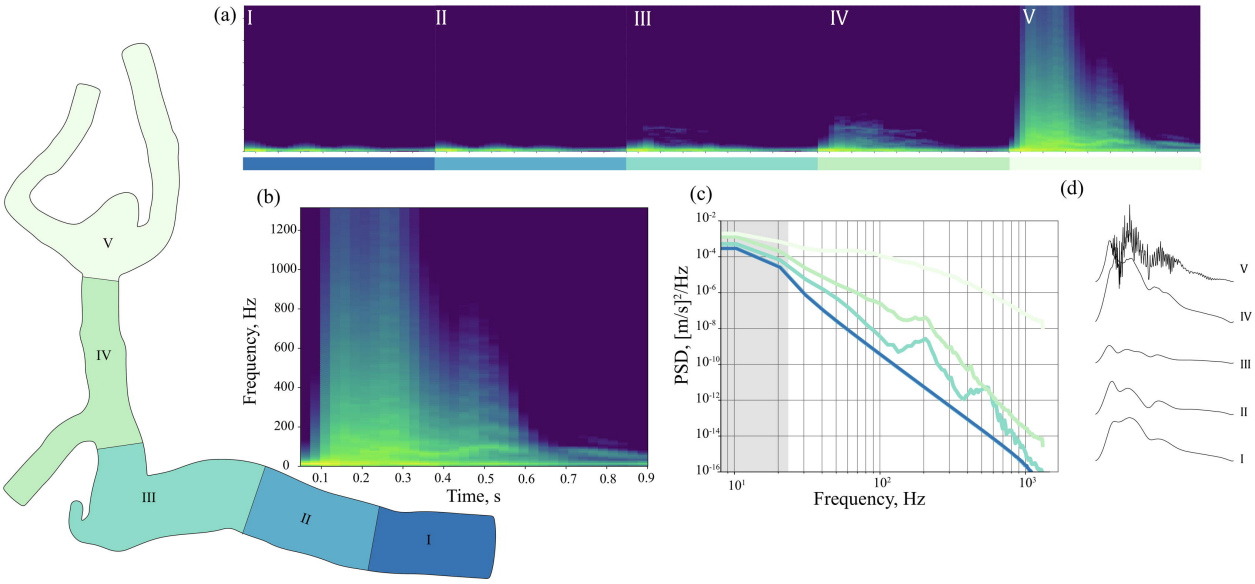

Figure 4: Local and global spectrograms for an aneurysm model (Case 0078 from AneuriskWeb project database): Regions (I-V) are shown colour-coded at left, with individual panels showing: (a) Local spectrograms derived from STFT power spectra averaged over the respective region; (b) global spectrogram derived from STFT power spectra averaged over whole model; (c) regional power-spectral density derived from simple FFT, and (d) velocity magnitude from a random Eulerian location in each of the sub-regions.

as a preprocessing step. Analogous to the wall filter in spectral Doppler, filtering out the low-frequency pulsatile inflow waveform can reduce the dynamic range of power, consequently the range of colour intensities, making the spectrogram more legible (e.g., compare Fig. 5b and Fig. 5b to Fig. 5a). We also recommend that for aneurysms at least, since the bulk of the spectral signatures are generated in the sac, which is anyway of most clinical interest, spectrograms may be generated from the sac region alone. Note that this presumes a nominally uniform node density throughout the model, as in our cases; for non-uniform meshes, or to reduce the number of velocity data points (and hence computational load and/or data storage) for generating spectrograms, a suitable random under-sampling strategy can be employed [35].

3.3 Interpretation and implications

As shown earlier (cf. Fig. 2), the global spectrograms can provide a comprehensive yet short-hand representation of the overall spectral content in the model. However, it is also possible that the global spectrograms can smooth out interesting features in the sac, which is of most interest in the case of aneurysms. It is also instructive to understand the flow dynamics that give rise to the resulting distinct features in the spectrogram.

In Fig. 6, we show the local spectrograms at three different probe locations for five aneurysm cases. The first column shows the flow instabilities through Q-criterion (a widely used mathematical algorithm based on velocity gradients to extract vortex cores) along with the local regions in the sac from which the spectrograms were generated. The volumetric rendering of Q-criterion shown here are snapshots at peak systole from the supplementary animations[2] for each of these cases. On observing the gross flow patterns (see supplementary animations[2]) in C0012 and C0032, they exhibit a stable laminar like flow with almost no instabilities in the sac, although C0012 shows some minor clusters. C0004 shows flow structures even late into the cardiac cycle denoting strong turbulent-like behavior of the flow that is persistent for a significant part of the cardiac cycle. C0053 shows strong vortex shedding of the incoming jet and the flow patterns appear to be fairly localized. C0060 shows flow instabilities that are persistent through the early diastole and intermittent puffs appear much late into the cardiac cycle. The locations (shown as I, II, and III and marked with coloured circles) were chosen within the sac to demonstrate the variability in the spectrograms and flow phenotypes.

The Q-criterion visualization of C0004 shows a highly unstable turbulent-like flow with large-scale flow structures captured in all three regions within the sac. These organized structures, shedding at fairly regular intervals, are reflected as narrowband features in the local spectrograms, and since all three are not substantially different from the global

[2]https://doi.org/10.1016/j.jbiomech.2020.109977

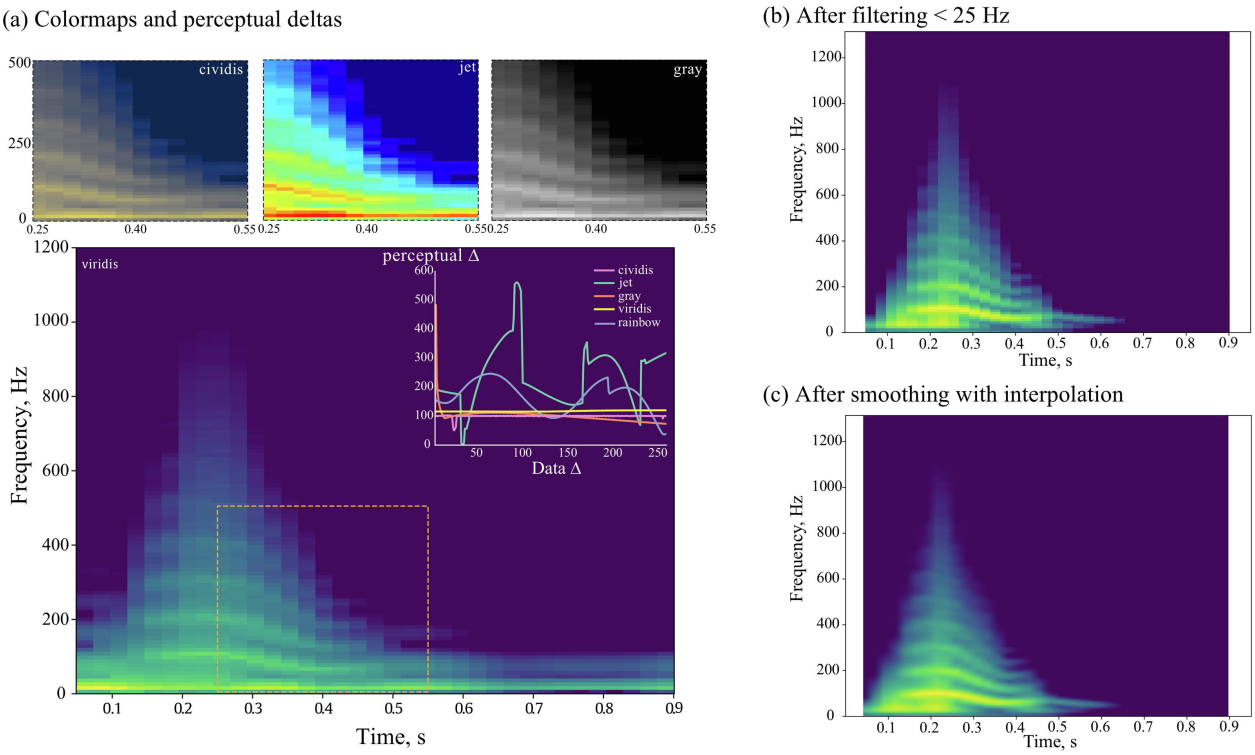

Figure 5: Effect of colourmap & dynamic range on spectrogram output for a carotid siphon model C0006 from Valen-Sendstad et al., 2014: (a) Spectrogram coloured using the perceptually optimized viridis colourmap (perceptually most uniform), showing also a portion of the spectrogram (see dashed box) coloured using other and standard colourmaps. Inset at the top right of the main spectrogram are the perceptual deltas of the various colourmaps, as discussed in the text; (b) spectrogram after filtering the (high-power) low frequencies below 25 Hz, and thus allowing more dynamic range for visualizing the higher frequencies; and (c) preservation of narrowband structures even after smoothing and interpolation of the visually-distracting discrete bins.

spectrogram for this case shown in Fig. 2, it is suggestive that the bulk contribution to the spectral content primarily arises from the sac in C0004. This is contrary to C0012, where the local spectrograms in the sac are different when compared to the global spectrogram of this model because, although not shown here, it had significant flow instabilities in the outflow branch bifurcation, distal to the sac (I, II a/o III). Despite being a giant aneurysm, C0012 does not show any significant (perhaps weak) flow instabilities in the sac (I, II a/o III). Where moderate flow instabilities are present (region II), they are reflected as weak striations up to $\sim$400 Hz. These local spectrograms show that the sac is dominated by the low-frequency inflow carrier. This is also true for C0032 where all regions within the sac are void of any high-frequency vortical structures throughout the cardiac cycle. C0053 shows regions of both turbulent-like flow instabilities (II) as well as regions of stasis (I & III). The spectrogram from the path of the incoming jet (II) captures the jet instability, the fluctuations from the shear layer, and the subsequent shedding exhibited as narrowband features in the spectrogram. Regions I & III in the recirculation zones of the sac pick up moderate flow fluctuations, albeit with weaker power when compared to region III. Region I, being in a secondary recirculation zone, only shows stable flow. Region I and II of C0060 are in the midst of the instabilities and as a result, share a near similar spectrogram. Both the regions experience persistent flow instabilities up until $\sim$0.35 s and a puff of instabilities again reappear at 0.5 s with a brief pause between the two events. These events are registered as broadband peaks in the spectrogram. Region III near the ostium is void of any strong flow structures, however, also being close to the regions of strong fluctuations (I and II), reflects the events (moderately) that take place in regions I and II.

4 Conclusion

Whether generated from STFT or CWT, the TFRs shown here provide a rich assessment of the spectral content in focal regions of cardiovascular models. In clinical workflows, the STFT may be a better candidate as it is relatively

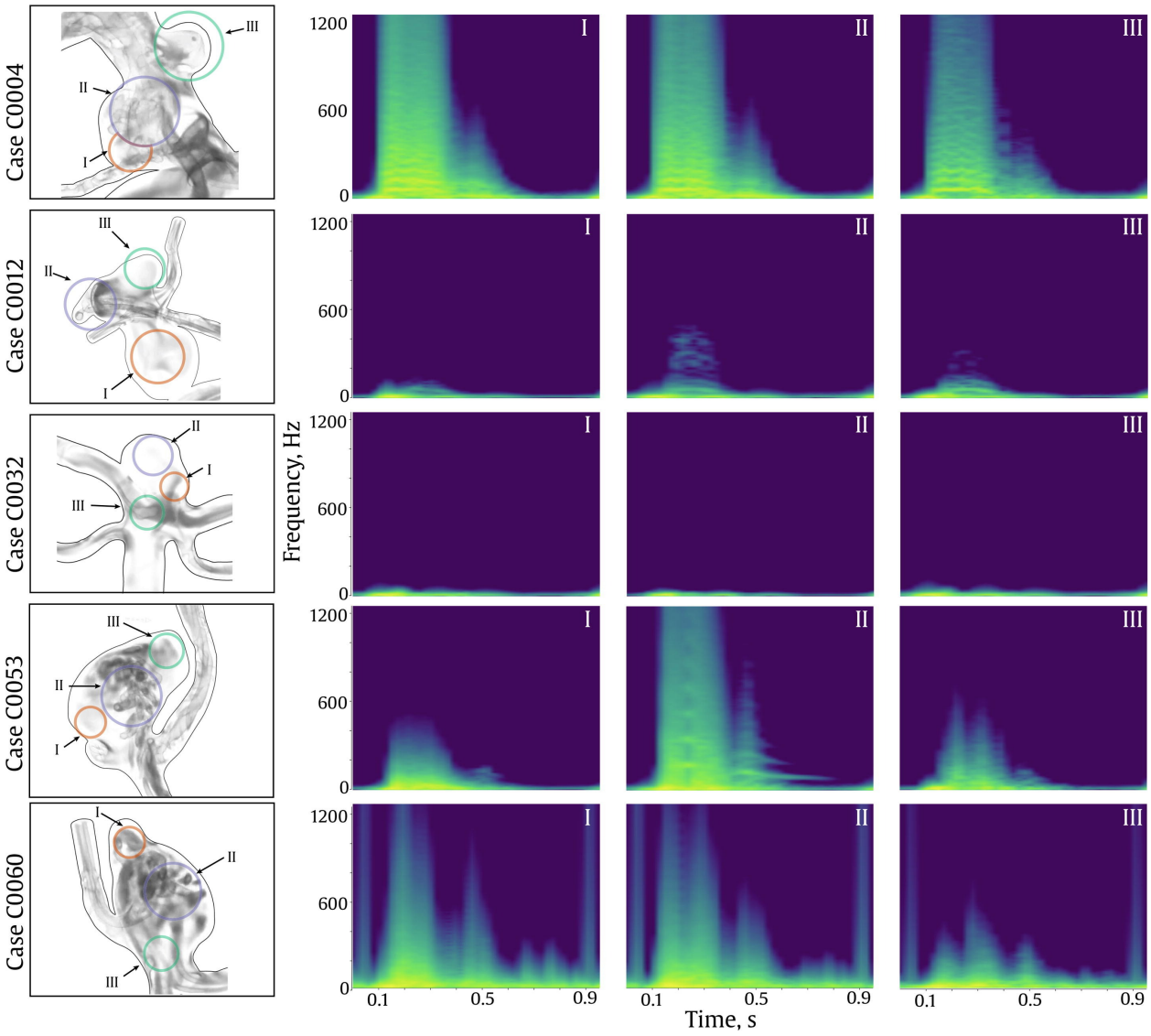

Figure 6: Effect of flow instabilities on local spectrograms for five aneurysm cases (Cases 0004, 0012, 0032, 0053 and 0060 from AneuriskWeb project database): Regions I, II and III to select points within their volume to compute the local spectrograms (row wise for each case). Supplementary animations show the spatiotemporal evolution of these flow instabilities in greater detail.[3]

simple, computationally inexpensive, and is structurally representative of its multiresolution counterpart, the CWT. Being fundamentally similar to Doppler spectrograms, they are also easier to explain and interpret for clinical readers.

The TFRs provide a comprehensive yet short-hand representation of the spectral content, which may potentially be used to discern unstable flow features that, in a research setting, might ultimately be associated with normal vs. pathological responses of the wall [5] or, in a clinical setting [8], with risk assessment or treatment planning. These render spectrograms a potentially useful and important tool to visualize and delineate the frequency contents and complexity of flow fluctuations in a compact and familiar form that may be attractive to researchers and clinicians alike.

5 Acknowledgements

The authors thank the anonymous reviewers, whose constructive comments helped us to improve the article significantly. Computations were performed on the Niagara supercomputer at the SciNet HPC Consortium. SciNet is funded by: the Canada Foundation for Innovation; the Government of Ontario; Ontario Research Fund—Research Excellence; and the University of Toronto.

6 Funding

This work is supported by a grant to D.A.S from the Natural Sciences and Engineering Research Council of Canada (RGPIN-2018-04649).

7 Appendix A. Supplementary material

Supplementary data to this article can be found online at https://doi.org/10.1016/j.jbiomech.2020.109977

References

[1] C. Chnafa, S. Mendez, and F. Nicoud. “Image-Based Simulations Show Important Flow Fluctuations in a Normal Left Ventricle: What Could be the Implications?” In: *Annals of Biomedical Engineering* 44.11 (Nov. 2016), pp. 3346–3358. DOI: 10.1007/s10439-016-1614-6.

[2] M. Bozzetto, B. Ene-Iordache, and A. Remuzzi. “Transitional Flow in the Venous Side of Patient-Specific Arteriovenous Fistulae for Hemodialysis”. In: *Annals of Biomedical Engineering* 44.8 (Aug. 2016), pp. 2388–2401. DOI: 10.1007/s10439-015-1525-y.

[3] V. Mancini et al. “High-Frequency Fluctuations in Post-stenotic Patient Specific Carotid Stenosis Fluid Dynamics: A Computational Fluid Dynamics Strategy Study”. In: *Cardiovascular Engineering and Technology* 10.2 (June 2019), pp. 277–298. DOI: 10.1007/s13239-019-00410-9.

[4] K. Valen-Sendstad et al. “Direct numerical simulation of transitional flow in a patient-specific intracranial aneurysm”. In: *Journal of Biomechanics* 44.16 (Nov. 2011), pp. 2826–2832. DOI: 10.1016/j.jbiomech.2011.08.015.

[5] P. F. Davies et al. “Turbulent fluid shear stress induces vascular endothelial cell turnover in vitro.” In: *Proceedings of the National Academy of Sciences* 83.7 (Apr. 1986), pp. 2114–2117. DOI: 10.1073/pnas.83.7.2114.

[6] D. R. Boughner and M. R. Roach. “Effect of Low Frequency Vibration on the Arterial Wall”. In: *Circulation Research* 29.2 (Aug. 1971), pp. 136–144. DOI: 10.1161/01.RES.29.2.136.

[7] A. I. Barakat. “Blood flow and arterial endothelial dysfunction: Mechanisms and implications”. In: *Comptes Rendus Physique* 14.6 (June 2013), pp. 479–496. DOI: 10.1016/j.crhy.2013.05.003.

[8] J. Cebral et al. “Flow Conditions in the Intracranial Aneurysm Lumen Are Associated with Inflammation and Degenerative Changes of the Aneurysm Wall”. In: *American Journal of Neuroradiology* 38.1 (Jan. 2017), pp. 119–126. DOI: 10.3174/ajnr.A4951.

[9] K. Taira et al. “Modal Analysis of Fluid Flows: An Overview”. In: *AIAA Journal* 55.12 (Dec. 2017), pp. 4013–4041. DOI: 10.2514/1.J056060.

[10] C. W. Rowley et al. “Spectral analysis of nonlinear flows”. In: *Journal of Fluid Mechanics* 641 (Dec. 2009), pp. 115–127. DOI: 10.1017/S0022112009992059.

[11] K. K. Chen, J. H. Tu, and C. W. Rowley. “Variants of Dynamic Mode Decomposition: Boundary Condition, Koopman, and Fourier Analyses”. In: *Journal of Nonlinear Science* 22.6 (Dec. 2012), pp. 887–915. DOI: 10.1007/s00332-012-9130-9.

[12] H. Witte et al. "Analysis and modeling of time-variant amplitude–frequency couplings of and between oscillations of EEG bursts". In: *Biological Cybernetics* 99.2 (Aug. 2008), pp. 139–157. DOI: 10.1007/s00422-008-0245-x.

[13] Y. Zhang et al. "A comparison of the wavelet and short-time fourier transforms for Doppler spectral analysis". In: *Medical Engineering & Physics* 25.7 (Sept. 2003), pp. 547–557. DOI: 10.1016/S1350-4533(03)00052-3.

[14] D. Komorowski and S. Pietraszek. "The Use of Continuous Wavelet Transform Based on the Fast Fourier Transform in the Analysis of Multi-channel Electrogastrography Recordings". In: *Journal of Medical Systems* 40.1 (Jan. 2016), p. 10. DOI: 10.1007/s10916-015-0358-4.

[15] G. Di Labbio, J. Vétel, and L. Kadem. "Material transport in the left ventricle with aortic valve regurgitation". In: *Physical Review Fluids* 3.11 (Nov. 2018), p. 113101. DOI: 10.1103/PhysRevFluids.3.113101.

[16] K. Valen-Sendstad, M. Piccinelli, and D. A. Steinman. "High-resolution computational fluid dynamics detects flow instabilities in the carotid siphon: Implications for aneurysm initiation and rupture?" In: *Journal of Biomechanics* 47.12 (Sept. 2014), pp. 3210–3216. DOI: 10.1016/j.jbiomech.2014.04.018.

[17] K. Valen-Sendstad and D. Steinman. "Mind the Gap: Impact of Computational Fluid Dynamics Solution Strategy on Prediction of Intracranial Aneurysm Hemodynamics and Rupture Status Indicators". In: *American Journal of Neuroradiology* 35.3 (Mar. 2014), pp. 536–543. DOI: 10.3174/ajnr.A3793.

[18] M. Wacker and H. Witte. "Time-frequency Techniques in Biomedical Signal Analysis: A Tutorial Review of Similarities and Differences". In: *Methods of Information in Medicine* 52.04 (2013), pp. 279–296. DOI: 10.3414/ME12-01-0083.

[19] D. Iatsenko, P. V. McClintock, and A. Stefanovska. "Linear and synchrosqueezed time–frequency representations revisited: Overview, standards of use, resolution, reconstruction, concentration, and algorithms". In: *Digital Signal Processing* 42 (July 2015), pp. 1–26. DOI: 10.1016/j.dsp.2015.03.004.

[20] Aneurisk-Team. *AneuriskWeb*. 2012. URL: http://ecm2.mathcs.emory.edu/aneuriskweb/index (visited on 06/29/2022).

[21] T. Natarajan et al. "Spectral decomposition and illustration-inspired visualisation of highly disturbed cerebrovascular blood flow dynamics". In: *Computer Methods in Biomechanics and Biomedical Engineering: Imaging & Visualization* 8.2 (Mar. 2020), pp. 182–193. DOI: 10.1080/21681163.2019.1647461.

[22] M. O. Khan, K. Valen-Sendstad, and D. A. Steinman. "Narrowing the Expertise Gap for Predicting Intracranial Aneurysm Hemodynamics: Impact of Solver Numerics versus Mesh and Time-Step Resolution". In: *American Journal of Neuroradiology* 36.7 (July 2015), pp. 1310–1316. DOI: 10.3174/ajnr.A4263.

[23] G. G. Ferguson. "Turbulence in human intracranial saccular aneurysms". In: *Journal of Neurosurgery* 33.5 (Nov. 1970), pp. 485–497. DOI: 10.3171/jns.1970.33.5.0485.

[24] Y Kurokawa, S Abiko, and K Watanabe. "Noninvasive detection of intracranial vascular lesions by recording blood flow sounds." In: *Stroke* 25.2 (Feb. 1994), pp. 397–402. DOI: 10.1161/01.STR.25.2.397.

[25] F. Harris. "On the use of windows for harmonic analysis with the discrete Fourier transform". In: *Proceedings of the IEEE* 66.1 (Jan. 1978), pp. 51–83. DOI: 10.1109/PROC.1978.10837.

[26] P. Avitabile. *Modal Testing: A Practitioner's Guide: A Practitioner's Guide*. Chichester, UK: John Wiley & Sons Ltd, Nov. 2017. DOI: 10.1002/9781119222989. URL: http://doi.wiley.com/10.1002/9781119222989 (visited on 06/23/2022).

[27] J. Allen. "Short term spectral analysis, synthesis, and modification by discrete Fourier transform". In: *IEEE Transactions on Acoustics, Speech, and Signal Processing* 25.3 (June 1977), pp. 235–238. DOI: 10.1109/TASSP.1977.1162950.

[28] S. S. Varghese, S. H. Frankel, and P. F. Fischer. "Direct numerical simulation of stenotic flows. Part 1. Steady flow". In: *Journal of Fluid Mechanics* 582 (July 2007), pp. 253–280. DOI: 10.1017/S0022112007005848.

[29] M. O. Khan et al. "On the quantification and visualization of transient periodic instabilities in pulsatile flows". In: *Journal of Biomechanics* 52 (Feb. 2017), pp. 179–182. DOI: 10.1016/j.jbiomech.2016.12.037.

[30] M. Borkin et al. "Evaluation of Artery Visualizations for Heart Disease Diagnosis". In: *IEEE Transactions on Visualization and Computer Graphics* 17.12 (Dec. 2011), pp. 2479–2488. DOI: 10.1109/TVCG.2011.192.

[31] K. Moreland. "Diverging Color Maps for Scientific Visualization". In: *Advances in Visual Computing*. Ed. by D. Hutchison et al. Vol. 5876. Berlin, Heidelberg: Springer Berlin Heidelberg, 2009, pp. 92–103. DOI: 10.1007/978-3-642-10520-3_9. URL: http://link.springer.com/10.1007/978-3-642-10520-3_9 (visited on 06/23/2022).

[32] J. R. Nuñez, C. R. Anderton, and R. S. Renslow. "Optimizing colormaps with consideration for color vision deficiency to enable accurate interpretation of scientific data". In: *PLOS ONE* 13.7 (Aug. 2018). Ed. by J. Malo, e0199239. DOI: 10.1371/journal.pone.0199239.

[33] S. van der Walt and N. Smith. *matplotlib colormaps*. URL: https://bids.github.io/colormap/ (visited on 06/23/2022).

[34] *Parula colormap array - MATLAB parula*. URL: https://www.mathworks.com/help/matlab/ref/parula.html (visited on 06/23/2022).

[35] D. Nehab and P. Shilane. "Stratified Point Sampling of 3D Models". In: *SPBG'04 Symposium on Point - Based Graphics 2004* (2004), 8 pages. DOI: 10.2312/SPBG/SPBG04/049-056.